nanomaterials

MDPI

Article

Visible Light Driven Heterojunction Photocatalyst of CuO–Cu_2O Thin Films for Photocatalytic Degradation of Organic Pollutants

Negar Dasineh Khiavi [1,†], Reza Katal [2,†], Saeideh Kholghi Eshkalak [3], Saeid Masudy-Panah [4], Seeram Ramakrishna [3,*] and Hu Jiangyong [2,*]

1 Faculty of Biosciences & Medical Engineering, University Technology Malaysia, Johor 81310, Malaysia
2 Department of Civil & Environmental Engineering, National University of Singapore, Singapore 119260, Singapore
3 Department of Mechanical Engineering, Center for Nanofibers and Nanotechnology, National University of Singapore, Singapore 117575, Singapore
4 Electrical and Computer Engineering, National University of Singapore, Singapore 119260, Singapore
* Correspondence: seeram@nus.edu.sg (S.R.); ceehujy@nus.edu.sg (H.J.)
† These authors contributed equally to this work.

Received: 22 June 2019; Accepted: 12 July 2019; Published: 13 July 2019

Abstract: A high recombination rate and low charge collection are the main limiting factors of copper oxides (cupric and cuprous oxide) for the photocatalytic degradation of organic pollutants. In this paper, a high performance copper oxide photocatalyst was developed by integrating cupric oxide (CuO) and cuprous oxide (Cu_2O) thin films, which showed superior performance for the photocatalytic degradation of methylene blue (MB) compared to the control CuO and Cu_2O photocatalyst. Our results show that a heterojunction photocatalyst of CuO–Cu_2O thin films could significantly increase the charge collection, reduce the recombination rate, and improve the photocatalytic activity.

Keywords: photocatalytic degradation; CuO; Cu_2O; heterojunction

1. Introduction

Rapidly increasing concentrations of organic pollutants such as pesticides, personal care products, and pharmaceuticals into different kinds of water sources have widely increased concerns over the potential impacts of these pollutants [1–3]. Conventional wastewater and water treatment cannot effectively remove organic pollutants due to their low biodegradability [4,5]. As a result, these pollutants are considered a serious threat to aquatic ecosystems and public health [6–9].

Different methods such as the heterogeneous photocatalytic process [10,11], heterogeneous catalytic oxidation with H_2O_2 [12], Fenton/photo-Fenton oxidation [13,14], ozonation [15], and UV/H_2O_2 treatment [16,17] can be used to destroy organic pollutants. Among these methods, the heterogeneous photocatalytic process is the most promising technique to remove organic pollutants from aqueous solutions because of its reusability, long term applicability, and low maintenance [18,19]. Due to the excellent chemical and physical characteristics of transition metal oxides, these materials are promising candidates in fabricating photocatalysts [20–26].

Both CuO and Cu_2O are considered as the most attractive photocatalysts for the photodegradation of organic pollutants due to their low fabrication cost, high optical absorption, and optimal optical bandgap for visible driven photocatalytic activity [27–30]. CuO and Cu_2O are the two main types of copper oxide. CuO is an indirect bandgap semiconductor with an optical absorption depth of around 500 nm, an optical bandgap of 1.7 eV, and a carrier diffusion length of around 200 nm, while Cu_2O

is a direct bandgap semiconductor with an optical absorption depth of around 1000 nm, an optical bandgap of 2.1 eV, and a carrier diffusion length of around 500 nm [31–35].

Various methods such as spin coating, electrochemical deposition, deep coating, electron beam evaporation, and sputter deposition can be used to prepare the thin film of CuO and Cu_2O. Among the different deposition methods of copper oxide, sputter deposition has the highest industrial compatibility, scalability, and repeatability [36–41].

Several studies have reported the application of CuO and Cu_2O for the photocatalytic degradation of organic pollutants in aqueous media. The CuO/zeoliteX was used for the photocatalytic degradation of methylene blue and o-phenylenediamine under sunlight irradiation [42,43]. CuO/SiO_2 was successfully used for MB degradation in a system under UV irradiation and in the presence of hydrogen peroxide [44]. In one study, the synthesis of the Cu_2O/carbon nanotubes was reported, which indicated considerable photocatalytic activity in phenol degradation in an aqueous solution [45]. Katal et al. reported the preparation of a high-efficient thin CuO film by in situ thermal treatment and nanocrystal engineering that indicated superior photocatalytic activity for MB degradation under visible light irradiation [23]. The considerable reusability and stability of this photocatalyst provide a new option for thin film based photocatalysts for industrial applications [23]. In another study, the fabrication of nanocrystalline CuO thin films was performed using RF magnetron sputtering; based on some special properties of this photocatalyst including surface defects and oxygen vacancy, the CuO thin film indicated remarkable photocatalytic performance for MB degradation [46].

The significant difference between carrier diffusion length and optical absorption depth is one of the main reasons for the high recombination rate and low charge collection of both the CuO and Cu_2O photocatalysts. Therefore, it is of great interest to develop a copper oxide photocatalyst in a way that reduces the recombination rate and increases the charge collection efficiency. In this paper, by integrating Cu_2O and CuO thin films, we prepared a heterojunction photocatalyst CuO–Cu_2O thin film with a low recombination rate and an enhanced charge collection to improve the photocatalytic activity of copper oxides.

2. Materials and Methods

All instruments (Singapore) used in this study for sample characterization were the same as those in our pervious publication [23]. Stoichiometric CuO and Cu_2O targets were used to deposit thin films of Cu_2O and CuO. All deposition was performed at a radio frequency sputtering power of 200 W and working pressure of 3 mTorr. Glass and fluorine doped tin oxide (FTO) coated glass substrates were used to prepare the samples.

Incident photon-to-current efficiency (IPCE) was carried out under standard light illumination of 300 W from a xenon lamp with an integrated parabolic reflector.

The photocatalytic degradation process is as completely described in our previous study [23]. A 300 W xenon lamp with a cut-off filter was used as the visible light source.

3. Results and Discussion

The cross-sectional transmission electron microscopy (CS-TEM) image of the fabricated CuO–Cu_2O photocatalyst is presented in Figure 1a. The overall thickness of the copper oxide photocatalyst was around 500 nm, which is similar to the carrier diffusion length of Cu_2O and the optical absorption depth of CuO. In addition, the thickness of the CuO thin layer was around 200 nm, which is similar to the carrier diffusion length of CuO.

Due to the lower optical absorption of Cu_2O than CuO, a greater bandgap of Cu_2O (around 2.2 eV) than CuO (around 1.6 eV), and a longer carrier diffusion length of Cu_2O (around 500 nm) than CuO (around 200 nm), Cu_2O was deposited on top of the CuO thin films (Figure 1b). Indeed if CuO is deposited on Cu_2O, the majority of carriers may recombine and cannot reach the conducting electrode, which results in the reduction in the performance of the heterojunction CuO–Cu_2O photocatalyst.

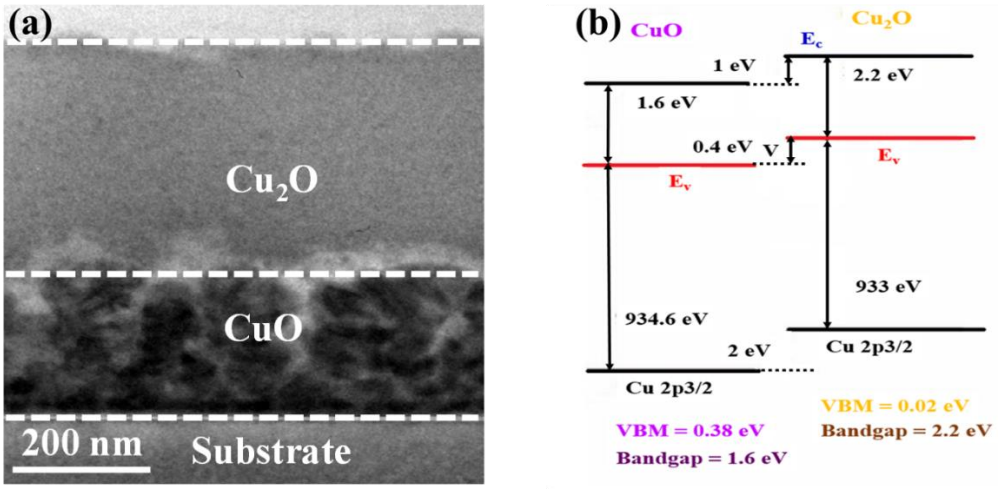

Figure 1. (**a**) Cross-sectional TEM image and (**b**) band alignment of the fabricated heterojunction CuO–Cu_2O thin film photocatalyst.

X-ray photoelectron spectroscopy (XPS) measurements were performed on top of each layer to verify the deposition of the CuO and Cu_2O thin film. Figure 2 shows the Cu2p XPS spectra of the bottom layer of CuO and the top layer of Cu_2O. Main XPS peaks at 933.9 eV were ascribed to the $2p_{3/2}$ peak of Cu^{2+}, indicating the deposition of CuO [47]. Shoulder peaks at higher binding energies further confirmed the deposition of CuO, while the main XPS peak at 932.5 eV corresponded to the $2p_{3/2}$ peak of Cu^{+}, confirming the deposition of the Cu_2O thin film [48,49].

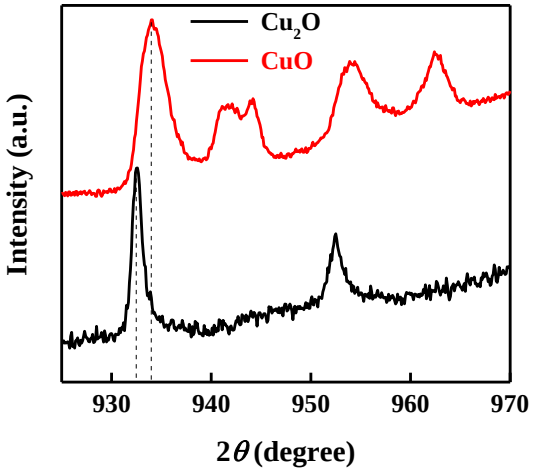

Figure 2. Cu2p XPS spectra of the bottom layer of CuO and the top layer of Cu_2O.

The XRD spectra of the prepared CuO–Cu_2O sample was measured to further investigate the material properties of the prepared photocatalyst. Figure 3 shows the XRD spectra of the CuO–Cu_2O thin films and the 500 nm CuO and Cu_2O control thin films. Main XRD peaks at 36.45 and 38.76 degrees were ascribed to Cu_2O(111) and CuO(111), respectively [5-667 and 5-661 JCPDS-ICDD]. As can be seen, in the CuO–Cu_2O sample, both XRD peaks of Cu_2O(111) and CuO(111) can be observed, indicating the existence of both kinds of copper oxides.

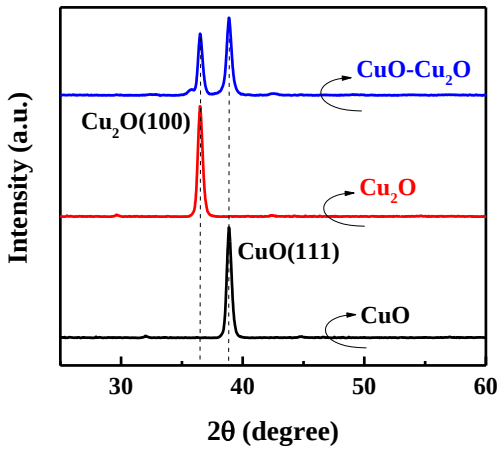

Figure 3. XRD spectra of the CuO–Cu_2O thin films and control CuO and Cu_2O thin films with a thickness of 500 nm.

To investigate the impact of the integration of CuO and Cu_2O on the optical properties of the fabricated photocatalyst, the optical absorption of the prepared samples was measured. Figure 4 shows the optical absorption of the heterojunction CuO–Cu_2O thin films as well as the control CuO and Cu_2O thin films with a thickness of around 500 nm. As can be seen, the integration of the Cu_2O and CuO thin films improved the optical absorption. Indeed, due to the different refractive index of Cu_2O (2.262) and CuO (2.654), the reflectance loss of the integrated CuO–Cu_2O was significantly reduced, hence optical absorption was improved according to the Equation (1) [50]:

$$R(\%) = (n_o - n_m)^2/(n_o + n_m)^2 \times 100, \quad (1)$$

where R, n_m, and n_o are reflectance in percentage, the refractive index of the underlying layer, and the refractive index of the top layer, respectively.

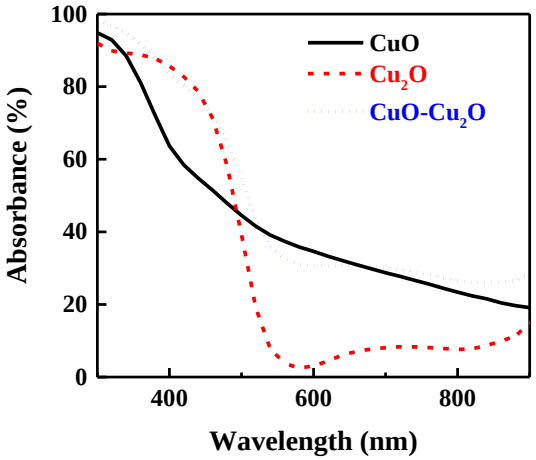

Figure 4. Absorbance spectra of the CuO, Cu_2O, and the heterojunction CuO–Cu_2O thin films.

The visible light driven photocatalytic activity of the Cu_2O, CuO, and CuO–Cu_2O thin films were investigated by considering the MB degradation. First, the MB degradation rate without photocatalysts under light irradiation and in the presence of a photocatalyst in the dark condition was studied; the results showed no considerable MB degradation rate, which clearly demonstrated that the MB degradation could only be possible in the presence of photocatalysts and visible light irradiation. To reach the adsorption equilibrium, the photocatalysts was placed in the MB solution under the dark condition for 30 min.

By proceeding with the photocatalytic reaction, the MB concentration gradually dropped due to the degradation reaction. The MB concentration change as a function of the photocatalytic degradation time was plotted and is shown in Figure 5a. In comparison with CuO and Cu_2O, the MB degradation rate by the CuO–Cu_2O sample was 0.0241 min^{-1}, which was almost twice that of the other samples. The images of the solution after degradation by CuO–Cu_2O are shown in Figure 5b; as can be seen, the solution color became light. This high photocatalytic activity of the CuO/Cu_2O sample can be considered as a suitable strategy for the elimination of organic pollutants from water and wastewater treatment systems at a large-scale.

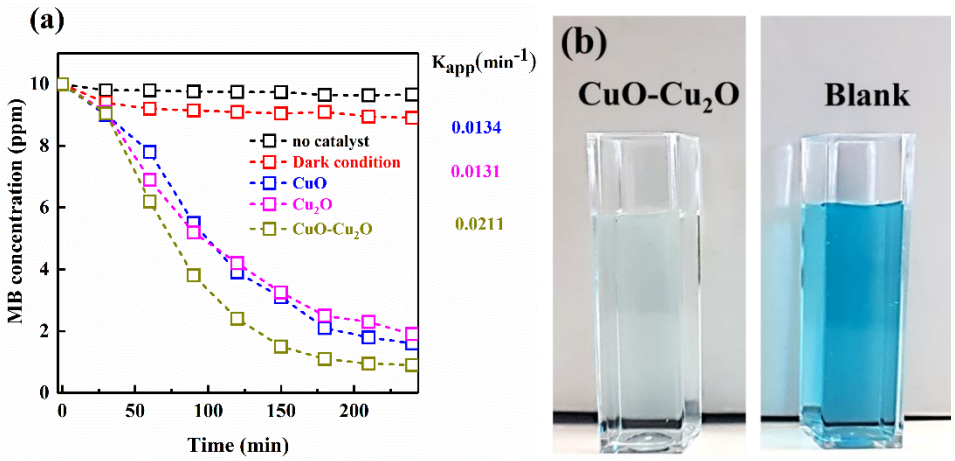

Figure 5. (**a**) Degradation profiles of MB vs. photocatalysis process time. (**b**) Images of the MB solution before and after photocatalysis by CuO–Cu_2O.

The superior visible-light driven photocatalytic activity of CuO–Cu_2O can be ascribed to its improved photo-generated charge carrier separation. Due to the presence of both types of copper oxides in the CuO–Cu_2O sample, the interface between these two copper oxides acted as a key parameter for the separation of the photo-generated electrons and holes [51,52]. Meanwhile, based on the difference in the energy levels of their CBs and VBs [53–55], this led to a higher absorption of visible light.

The charge collection efficiency of the prepared samples was evaluated by measuring the IPCE characteristics at 0 V versus RHE. Figure 6 illustrates the IPCE characteristics of the heterojunction CuO–Cu_2O thin films and the control CuO and Cu_2O thin films with a thickness of 500 nm. As can be seen, the IPCE of the heterojunction CuO–Cu_2O thin film was greater than that of the CuO and Cu_2O thin films over a broad range of wavelengths, indicating an improvement in the charge collection of integrated CuO–Cu_2O thin films when compared to the control CuO and Cu_2O samples.

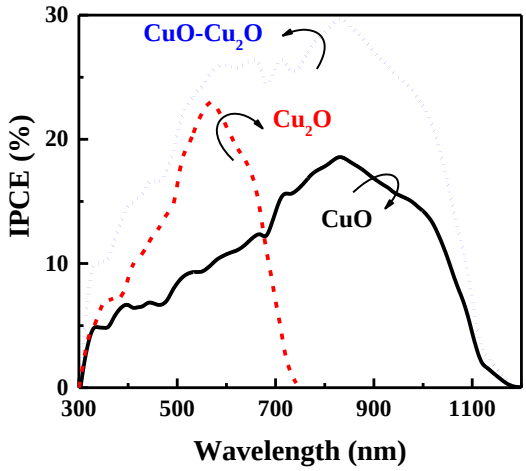

Figure 6. IPCE spectra of the CuO, Cu_2O, and heterojunction CuO–Cu_2O thin film photocatalysts.

Electrochemical impedance spectroscopy (EIS) was used to investigate the kinetics of the interfacial charge transfer of the prepared samples. The Nyquist plot of the prepared CuO–Cu_2O thin film as well as those of the CuO and Cu_2O control samples under standard solar illumination at the potential of 0 V vs. RHE is presented in Figure 7. The semi-circle nature of the Nyquist plot at high frequencies is indicative of the charge transfer process and the diameter of the semi-circle is indicative of the interfacial charge transfer resistance between the electrolyte and photocatalyst (R_{ct}). As seen in Figure 7, the integration of CuO and Cu_2O significantly reduced the R_{ct}, indicating an improvement in the charge transfer, a reduction in the recombination rate, and an improvement in photocatalytic activity. The trend of the R_{ct} values correlated well with the measured IPCE of the prepared samples.

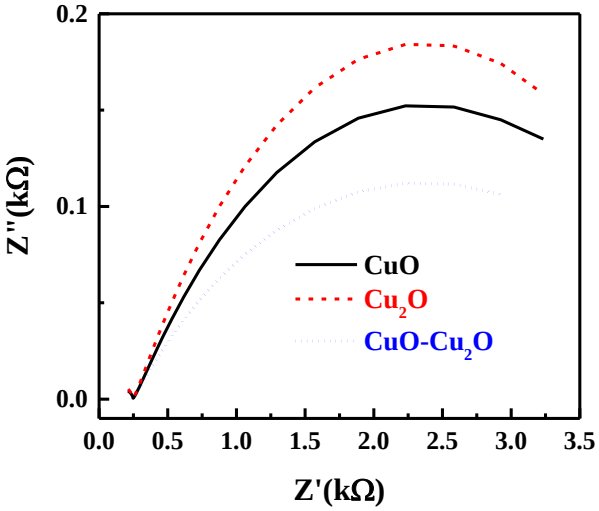

Figure 7. Nyquist plot of the CuO, Cu_2O and heterojunction CuO–Cu_2O thin film photocatalysts.

To further investigate the impact of the integration of Cu_2O and CuO on the performance of the prepared photocatalyst, linear voltammetry measurements were performed at the pH of the electrolyte of 5.2. Figure 8a,b show the photoelectrochemical (PEC) current density and the photocorrosion stability of the control CuO and Cu_2O photocatalysts and the CuO–Cu_2O photocatalyst, respectively. The thickness of the CuO and Cu_2O control photocatalysts was set at around 500 nm (similar to the thickness of the CuO–Cu_2O photocatalyst). The PEC current density was measured under dark and standard solar AM 1.5G illumination of 100 mW/cm^2 ("light on") conditions. Photocorrosion stability was measured at a potential of 0.25 V vs. RHE. Photocurrent and photocorrosion stability of a photocatalyst is generally determined by the recombination rate and charge collection efficiency. Enhanced photocurrent and photocorrosion stability of the CuO–Cu_2O photocatalyst when compared to the control CuO and Cu_2O photocatalysts indicates a reduction in the recombination rate and an enhancement in the separation of generated electron hole pairs. Furthermore, according to the measured PEC characteristics of the deposited CuO, Cu_2O, and CuO–Cu_2O thin films on FTO coated substrates, it can be concluded that fabricated electrodes behaved as photocathodes.

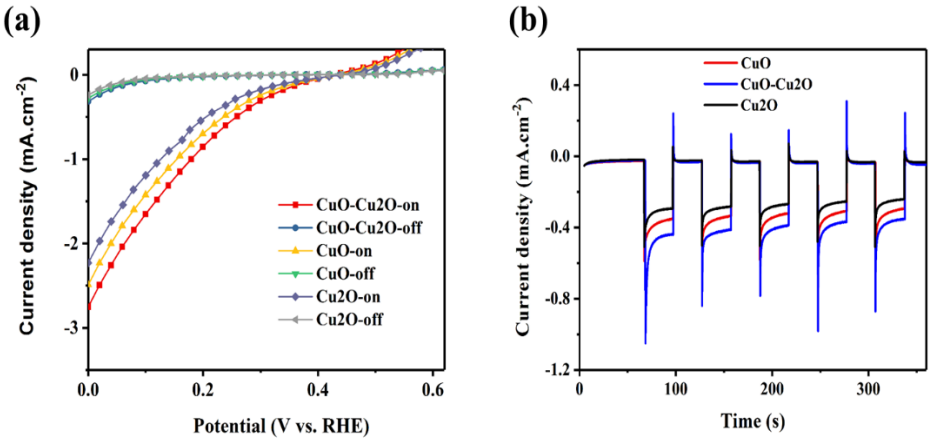

Figure 8. (**a**) photoelectrochemical (PEC) current density and (**b**) photocorrosion stability of the control CuO and Cu_2O photocatalysts and CuO–Cu_2O photocatalyst.

The CuO–Cu_2O photocatalysis mechanism (based on the CB & VB) are graphically presented in Figure 9. Due to the band gap values of Cu_2O (2.2 eV) and CuO (1.7 eV), both oxides have a high capacity to light absorption in the visible range and can subsequently generate a photo-generated electron-hole pair under visible light irradiation [56,57]. The band edge positions of materials in a heterojunction net strongly affect the photo-generated charge carrier transfer direction [58,59]. As shown in Figure 9, both the CB and VB of Cu_2O placed below those of CuO; therefore, the photo-generated electrons transfer took place from the Cu_2O transferred to the CB of CuO under visible light irradiation; whereas the photo-generated holes from CuO transferred to the VB of Cu_2O [60,61]. Therefore, due to the transfer of the photo-generated electrons and holes in the CuO–Cu_2O heterojunction net, a significant increase in the life-time of the photogenerated electron-hole pair was observed. $O_2^{\bullet -}$ and $OH^{\bullet}$, as highly oxidative radical species, were generated with the electrons captured by the adsorbed oxygen molecules and holes trapped by the surface hydroxyl, respectively.

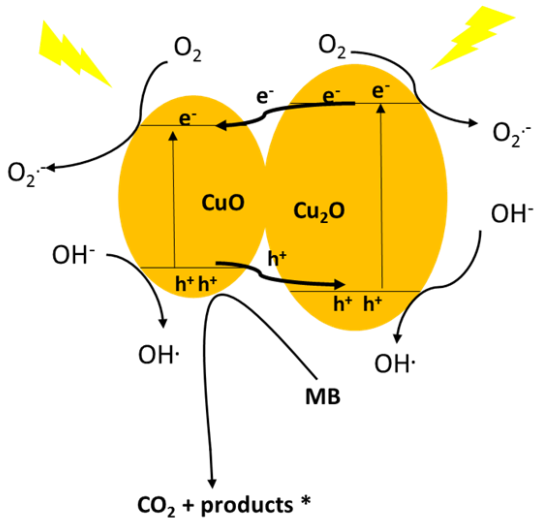

Figure 9. Proposed schematic illustration of the band structure related photocatalytic mechanism for the CuO–Cu_2O heterojunction net.

Generally, the degradation of organic pollutants by semiconductors in aqueous environments results from reactive oxygen species ($O_2^{\bullet -}$, H_2O_2, and $OH^{\bullet}$) and photogenerated hole (h^+) generation during light irradiation. The relevant reactions can be described as follows:

$$\text{CuO-Cu}_2\text{O} + h\nu \rightarrow e^- + h^+ \quad (2)$$

$$e^- + O_2 \rightarrow O_2^{\bullet -} \quad (3)$$

$$e^- + O_2^{\bullet -} + 2H^+ \rightarrow H_2O_2 \quad (4)$$

$$2e^- + HO_2^{\bullet} + H^+ \rightarrow OH^{\bullet} + OH^- \quad (5)$$

$$h^+, H_2O_2, O_2^{\bullet -}, OH^{\bullet} + MB \rightarrow \text{products } (CO_2, H_2O, SO_4^{-2}, NO_3^-, NH_4^+) \quad (6)$$

To investigate the role of ROSs in MB photocatalytic degradation, t-butanol (t-OH), ammonium oxalate (AO), catalase (CAT), and benzoquinone (BQ) were used as scavengers of the hydroxyl radicals ($OH^{\bullet}$), photo-generated holes (h^+), H_2O_2, and superoxide radicals ($O_2^{\bullet -}$), respectively [62]. The MB degradation efficiency by CuO–Cu_2O in the presence of scavengers is shown in Figure 10. As can be seen, an obvious reduction in the photocatalytic activity of CuO–Cu_2O was observed in the presence of the t-OH, BQ, and OA, which clearly showed the contribution of $OH^{\bullet}$, superoxide, and h^+ in the photocatalytic degradation process. However, by adding CAT as a scavenger of H_2O_2, a light reduction in degradation efficiency was observed; this obviously indicates that H_2O_2 did not play an important role in MB degradation by CuO–Cu_2O.

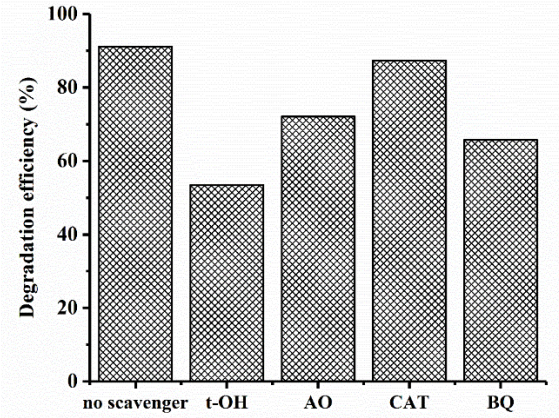

Figure 10. Effect of scavengers on the photocatalytic activity of CuO–Cu_2O.

To evaluate the capacity of CuO–Cu_2O for large-scale application, the reusability of this sample was tested for five cycles. Figure 11 presents the degradation rate from the five cycle tests. As can be seen, the degradation rate was repeatable. The reduction in photocatalytic degradation rate after five cycles was less than 5%.

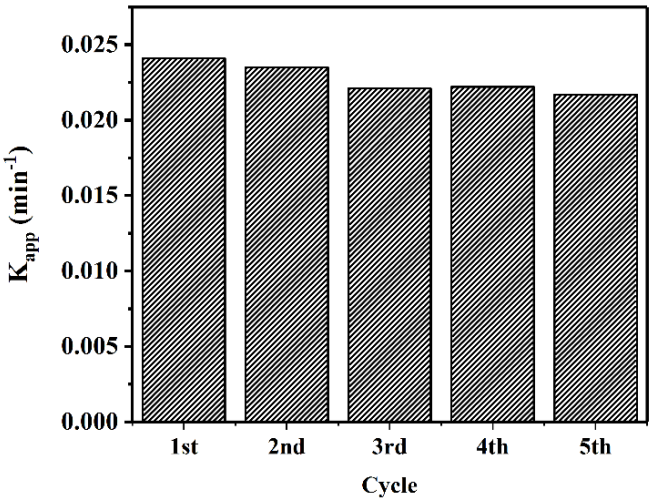

Figure 11. Reusability of the CuO–Cu_2O sample under visible light irradiation during MB degradation.

4. Conclusions

In conclusion, an efficient visible-light-driven heterojunction photocatalyst of CuO–Cu_2O thin films for the photocatalytic degradation of methylene blue was fabricated. It was shown that the integration of Cu_2O and CuO could significantly increase the charge collection and reduce the recombination rate inside the photocatalyst. Furthermore, it was found that integrating CuO and Cu_2O could improve the optical absorption and facilitate the charge transfer at the interface between the photocatalyst and electrolyte.

Author Contributions: Synthesis and experimental design, N.D.K. and R.K.; Sample characterization, R.K., S.M.P., and S.K.E.; Concentration analysis, R.K. and S.K.E.; Supervision, S.R. and H.J.; Writing—original draft, N.D.K. and R.K.; Writing—review & editing, H.J. and S.R.

Funding: This research received no external funding.

Acknowledgments: The authors acknowledge the financial support from the Singapore International Graduate Award (SINGA).

Conflicts of Interest: The authors declare no conflicts of interest.

References

1. Wu, L.; Wan, G.; Hu, N.; He, Z.; Shi, S.; Suo, Y.; Wang, K.; Xu, X.; Tang, Y.; Wang, G. Synthesis of Porous $CoFe_2O_4$ and Its Application as a Peroxidase Mimetic for Colorimetric Detection of H_2O_2 and Organic Pollutant Degradation. *Nanomaterials* **2018**, *8*, 451. [CrossRef] [PubMed]
2. Moreno-Castilla, C.; López-Ramón, M.V.; Fontecha-Cámara, M.Á.; Álvarez, M.A.; Mateus, L. Removal of Phenolic Compounds from Water Using Copper Ferrite Nanosphere Composites as Fenton Catalysts. *Nanomaterials* **2019**, *9*, 901. [CrossRef] [PubMed]
3. Chen, J.; Li, G.; Liu, Q.; Liang, Y.; Liu, M.; Wu, H.; Gao, W. A Photocleavable Amphiphilic Prodrug Self-Assembled Nanoparticles with Effective Anticancer Activity In Vitro. *Nanomaterials* **2019**, *9*, 860. [CrossRef] [PubMed]
4. Li, Q.; Wang, Q.; Chen, Z.; Ma, Q.; An, M. A Facile and Flexible Approach for Large-Scale Fabrication of ZnO Nanowire Film and Its Photocatalytic Applications. *Nanomaterials* **2019**, *9*, 846. [CrossRef] [PubMed]
5. Long, X.; Ren, J.; Zhang, C.; Ji, F.; Jia, L. Facile and Controllable Fabrication of Protein-Only Nanoparticles through Photo-Induced Crosslinking of Albumin and Their Application as DOX Carriers. *Nanomaterials* **2019**, *9*, 797. [CrossRef] [PubMed]
6. Sun, Y.; Qu, B.; Liu, Q.; Gao, S.; Yan, Z.; Yan, W.; Pan, B.; Wei, S.; Xie, Y. Highly efficient visible-light-driven photocatalytic activities in synthetic ordered monoclinic $BiVO_4$ quantum tubes–graphene nanocomposites. *Nanoscale* **2012**, *4*, 3761. [CrossRef] [PubMed]
7. Chang, C.-T.; Wang, J.-J.; Ouyang, T.; Zhang, Q.; Jing, Y.-H. Photocatalytic degradation of acetaminophen in aqueous solutions by TiO2/ZSM-5 zeolite with low energy irradiation. *Mater. Sci. Eng. B* **2015**, *196*, 53–60. [CrossRef]
8. Sun, K.; Wang, L.; Wu, C.; Deng, J.; Pan, K. Fabrication of α-Fe_2O_3@rGO/PAN Nanofiber Composite Membrane for Photocatalytic Degradation of Organic Dyes. *Adv. Mater. Interfaces* **2017**, *4*, 1700845. [CrossRef]
9. Kümmerer, K. Drugs in the environment: Emission of drugs, diagnostic aids and disinfectants into wastewater by hospitals in relation to other sources—A review. *Chemosphere* **2001**, *45*, 957–969. [CrossRef]
10. Calza, P.; Sakkas, V.; Medana, C.; Baiocchi, C.; Dimou, A.; Pelizzetti, E.; Albanis, T. Photocatalytic degradation study of diclofenac over aqueous TiO_2 suspensions. *Appl. Catal. B Environ.* **2006**, *67*, 197–205. [CrossRef]
11. Rizzo, L.; Meric, S.; Kassinos, D.; Guida, M.; Russo, F.; Belgiorno, V. Degradation of diclofenac by TiO_2 photocatalysis: UV absorbance kinetics and process evaluation through a set of toxicity bioassays. *Water Res.* **2009**, *43*, 979–988. [CrossRef] [PubMed]
12. Hofmann, J.; Freier, U.; Wecks, M.; Hohmann, S. Degradation of diclofenac in water by heterogeneous catalytic oxidation with H_2O_2. *Appl. Catal. B Environ.* **2007**, *70*, 447–451. [CrossRef]
13. Klamerth, N.; Rizzo, L.; Malato, S.; Maldonado, M.I.; Agüera, A.; Fernández-Alba, A.R. Degradation of fifteen emerging contaminants at μgL−1 initial concentrations by mild solar photo-Fenton in MWTP effluents. *Water Res.* **2010**, *44*, 545–554. [CrossRef] [PubMed]

14. Pérez-Estrada, L.A.; Maldonado, M.I.; Gernjak, W.; Agüera, A.; Fernández-Alba, A.R.; Ballesteros, M.M.; Malato, S. Decomposition of diclofenac by solar driven photocatalysis at pilot plant scale. *Catal. Today* **2005**, *101*, 219–226. [CrossRef]
15. Vogna, D.; Marotta, R.; Napolitano, A.; Andreozzi, R.; D'Ischia, M. Advanced oxidation of the pharmaceutical drug diclofenac with UV/H2O2 and ozone. *Water Res.* **2004**, *38*, 414–422. [CrossRef] [PubMed]
16. Klavarioti, M.; Mantzavinos, D.; Kassinos, D. Removal of residual pharmaceuticals from aqueous systems by advanced oxidation processes. *Environ. Int.* **2009**, *35*, 402–417. [CrossRef]
17. Kim, I.; Yamashita, N.; Tanaka, H. Performance of UV and UV/H_2O_2 processes for the removal of pharmaceuticals detected in secondary effluent of a sewage treatment plant in Japan. *J. Hazard. Mater.* **2009**, *166*, 1134–1140. [CrossRef]
18. Paracchino, A.; Laporte, V.; Sivula, K.; Grätzel, M.; Thimsen, E. Highly active oxide photocathode for photoelectrochemical water reduction. *Nat. Mater.* **2011**, *10*, 456–461. [CrossRef]
19. Morales-Guio, C.G.; Tilley, S.D.; Vrubel, H.; Grätzel, M.; Hu, X. Hydrogen evolution from a copper(I) oxide photocathode coated with an amorphous molybdenum sulphide catalyst. *Nat. Commun.* **2014**, *5*, 3059. [CrossRef]
20. López, R.; Gómez, R.; Llanos, M.E. Photophysical and photocatalytic properties of nanosized copper-doped titania sol–gel catalysts. *Catal. Today* **2009**, *148*, 103–108. [CrossRef]
21. Katal, R.; Salehi, M.; Davood Abadi Farahani, M.H.; Masudy-Panah, S.; Ong, S.L.; Hu, J. Preparation of a New Type of Black TiO_2 under a Vacuum Atmosphere for Sunlight Photocatalysis. *ACS Appl. Mater. Interfaces* **2018**, *10*, 35316–35326. [CrossRef]
22. Masudy-Panah, S.; Eugene, Y.-J.K.; Khiavi, N.D.; Katal, R.; Gong, X. Aluminum-incorporated p-CuO/n-ZnO photocathode coated with nanocrystal-engineered TiO_2 protective layer for photoelectrochemical water splitting and hydrogen generation. *J. Mater. Chem. A* **2018**, *6*, 11951–11965. [CrossRef]
23. Katal, R.; Masudy-panah, S.; Kong, E.Y.-J.; Dasineh Khiavi, N.; Abadi Farahani, M.H.D.; Gong, X. Nanocrystal-engineered thin CuO film photocatalyst for visible-light-driven photocatalytic degradation of organic pollutant in aqueous solution. *Catal. Today* **2018**. [CrossRef]
24. Katal, R.; Kholghi Eshkalak, S.; Masudy-panah, S.; Kosari, M.; Saeedikhani, M.; Zarinejad, M.; Ramakrishna, S. Evaluation of Solar-Driven Photocatalytic Activity of Thermal Treated TiO_2 under Various Atmospheres. *Nanomaterials* **2019**, *9*, 163. [CrossRef]
25. Katal, R.; Masudy Panah, S.; Zarinejad, M.; Salehi, M.; Jiangyong, H. Synthesis of Self-Gravity Settling Faceted-Anatase TiO_2 with Dominant {010} Facets for the Photocatalytic Degradation of Acetaminophen and Study of the Type of Generated Oxygen Vacancy in Faceted-TiO_2. *Water* **2018**, *10*, 1462. [CrossRef]
26. Katal, R.; Farahani, M.H.D.A.; Masudy-Panah, S.; Ong, S.L.; Hu, J. Polypyrrole- and polyaniline-supported TiO_2 for removal of pollutants from water. *J. Environ. Eng. Sci.* **2019**, *14*, 67–89. [CrossRef]
27. Petronella, F.; Truppi, A.; Dell'Edera, M.; Agostiano, A.; Curri, M.L.; Comparelli, R. Scalable Synthesis of Mesoporous TiO_2 for Environmental Photocatalytic Applications. *Materials* **2019**, *12*, 1853. [CrossRef]
28. Katal, R.; Panah, S.M.; Saeedikhani, M.; Kosari, M.; Sheng, C.C.; Leong, O.S.; Xiao, G.; Jiangyong, H. Pd-Decorated CuO Thin Film for Photodegradation of Acetaminophen and Triclosan under Visible Light Irradiation. *Adv. Mater. Interfaces* **2018**, *5*, 1801440. [CrossRef]
29. Lu, Y.; Liu, X.; Qiu, K.; Cheng, J.; Wang, W.; Yan, H.; Tang, C.; Kim, J.-K.; Luo, Y. Facile Synthesis of Graphene-Like Copper Oxide Nanofilms with Enhanced Electrochemical and Photocatalytic Properties in Energy and Environmental Applications. *ACS Appl. Mater. Interfaces* **2015**, *7*, 9682–9690. [CrossRef]
30. Yin, G.; Nishikawa, M.; Nosaka, Y.; Srinivasan, N.; Atarashi, D.; Sakai, E.; Miyauchi, M. Photocatalytic Carbon Dioxide Reduction by Copper Oxide Nanocluster-Grafted Niobate Nanosheets. *ACS Nano* **2015**, *9*, 2111–2119. [CrossRef]
31. Masudy-Panah, S.; Zhuk, S.; Tan, H.R.; Gong, X.; Dalapati, G.K. Palladium nanostructure incorporated cupric oxide thin film with strong optical absorption, compatible charge collection and low recombination loss for low cost solar cell applications. *Nano Energy* **2018**, *46*, 158–167. [CrossRef]
32. Masudy-Panah, S.; Kakran, M.; Lim, Y.-F.; Chua, C.S.; Tan, H.R.; Dalapati, G.K. Graphene nanoparticle incorporated CuO thin film for solar cell application. *J. Renew. Sustain. Energy* **2016**, *8*, 043507. [CrossRef]
33. Masudy-Panah, S.; Siavash Moakhar, R.; Chua, C.S.; Tan, H.R.; Wong, T.I.; Chi, D.; Dalapati, G.K. Nanocrystal Engineering of Sputter-Grown CuO Photocathode for Visible-Light-Driven Electrochemical Water Splitting. *ACS Appl. Mater. Interfaces* **2016**, *8*, 1206–1213. [CrossRef]

34. Luo, J.; Steier, L.; Son, M.-K.; Schreier, M.; Mayer, M.T.; Grätzel, M. Cu_2O Nanowire Photocathodes for Efficient and Durable Solar Water Splitting. *Nano Lett.* **2016**, *16*, 1848–1857. [CrossRef]
35. Musselman, K.P.; Marin, A.; Schmidt-Mende, L.; MacManus-Driscoll, J.L. Incompatible Length Scales in Nanostructured Cu_2O Solar Cells. *Adv. Funct. Mater.* **2012**, *22*, 2202–2208. [CrossRef]
36. Dalapati, G.K.; Kajen, R.S.; Masudy-Panah, S.; Sonar, P. Defect analysis of sputter grown cupric oxide for optical and electronics application. *J. Phys. D Appl. Phys.* **2015**, *48*, 495104. [CrossRef]
37. Masudy-Panah, S.; Siavash Moakhar, R.; Chua, C.S.; Kushwaha, A.; Dalapati, G.K. Stable and Efficient CuO Based Photocathode through Oxygen-Rich Composition and Au–Pd Nanostructure Incorporation for Solar-Hydrogen Production. *ACS Appl. Mater. Interfaces* **2017**, *9*, 27596–27606. [CrossRef]
38. Masudy-Panah, S.; Moakhar, R.S.; Chua, C.S.; Kushwaha, A.; Wong, T.I.; Dalapati, G.K. Rapid thermal annealing assisted stability and efficiency enhancement in a sputter deposited CuO photocathode. *RSC Adv.* **2016**, *6*, 29383–29390. [CrossRef]
39. Masudy-Panah, S.; Radhakrishnan, K.; Tan, H.R.; Yi, R.; Wong, T.I.; Dalapati, G.K. Titanium doped cupric oxide for photovoltaic application. *Sol. Energy Mater. Sol. Cells* **2015**, *140*, 266–274. [CrossRef]
40. Dalapati, G.K.; Masudy-Panah, S.; Chua, S.T.; Sharma, M.; Wong, T.I.; Tan, H.R.; Chi, D. Color tunable low cost transparent heat reflector using copper and titanium oxide for energy saving application. *Sci. Rep.* **2016**, *6*, 20182. [CrossRef]
41. Dalapati, G.K.; Batabyal, S.K.; Masudy-Panah, S.; Su, Z.; Kushwaha, A.; Wong, T.I.; Liu, H.F.; Bhat, T.; Iskander, A.; Lim, Y.-F.; et al. Sputter grown sub-micrometer thick Cu_2ZnSnS_4 thin film for photovoltaic device application. *Mater. Lett.* **2015**, *160*, 45–50. [CrossRef]
42. Nezamzadeh-Ejhieh, A.; Hushmandrad, S. Solar photodecolorization of methylene blue by CuO/X zeolite as a heterogeneous catalyst. *Appl. Catal. A* **2010**, *388*, 149–159. [CrossRef]
43. Nezamzadeh-Ejhieh, A.; Salimi, Z. Solar photocatalytic degradation of o-phenylenediamine by heterogeneous CuO/X zeolite catalyst. *Desalination* **2011**, *280*, 281–287. [CrossRef]
44. Batista, A.P.L.; Carvalho, H.W.P.; Luz, G.H.P.; Martins, P.F.; Gonçalves, M.; Oliveira, L.C. Preparation of CuO/SiO_2 and photocatalytic activity by degradation of methylene blue. *Environ. Chem. Lett.* **2010**, *8*, 63–67. [CrossRef]
45. Lufeng, Y.; Deqing, C.; Limin, W.; Xu, W.; Junya, L. Synthesis and photocatalytic activity of chrysanthemum-like Cu_2O/Carbon Nanotubes nanocomposites. *Ceram. Int.* **2016**, *42*, 2502–2509. [CrossRef]
46. Al-Ghamdi, A.A.; Khedr, M.H.; Ansari, M.S.; Hasan, P.M.Z.; Abdel-Wahab, M.S.; Farghali, A.A. RF sputtered CuO thin films: Structural, optical and photo-catalytic behavior. *Phys. E Low-Dimens. Syst. Nanostruct.* **2016**, *81*, 83–90. [CrossRef]
47. Balamurugan, B.; Mehta, B.R.; Shivaprasad, S.M. Surface-modified CuO layer in size-stabilized single-phase Cu_2O nanoparticles. *Appl. Phys. Lett.* **2001**, *79*, 3176–3178. [CrossRef]
48. Ghodselahi, T.; Vesaghi, M.A.; Shafiekhani, A.; Baghizadeh, A.; Lameii, M. XPS study of the $Cu@Cu_2O$ core-shell nanoparticles. *Appl. Surf. Sci.* **2008**, *255*, 2730–2734. [CrossRef]
49. Pauly, N.; Tougaard, S.; Yubero, F. Determination of the Cu 2p primary excitation spectra for Cu, Cu_2O and CuO. *Surf. Sci.* **2014**, *620*, 17–22. [CrossRef]
50. Kim, K.-C. Effective graded refractive-index anti-reflection coating for high refractive-index polymer ophthalmic lenses. *Mater. Lett.* **2015**, *160*, 158–161. [CrossRef]
51. Chen, J.; Nie, X.; Shi, H.; Li, G.; An, T. Synthesis of TiO_2 hollow sphere multimer photocatalyst by etching titanium plate and its application to the photocatalytic decomposition of gaseous styrene. *Chem. Eng. J.* **2013**, *228*, 834–842. [CrossRef]
52. Gao, F.; Feng, W.; Wei, G.; Zheng, J.; Wang, M.; Yang, W. Triangular prism-shaped p-type 6H-SiC nanowires. *CrystEngComm* **2012**, *14*, 488–491. [CrossRef]
53. Wang, S.L.; Li, P.G.; Zhu, H.W.; Tang, W.H. Controllable synthesis and photocatalytic property of uniform CuO/Cu_2O composite hollow microspheres. *Powder Technol.* **2012**, *230*, 48–53. [CrossRef]
54. Yu, H.; Yu, J.; Liu, S.; Mann, S. Template-free Hydrothermal Synthesis of CuO/Cu_2O Composite Hollow Microspheres. *Chem. Mater.* **2007**, *19*, 4327–4334. [CrossRef]
55. Liu, X.; Chen, J.; Liu, P.; Zhang, H.; Li, G.; An, T.; Zhao, H. Controlled growth of CuO/Cu_2O hollow microsphere composites as efficient visible-light-active photocatalysts. *Appl. Catal. A Gen.* **2016**, *521*, 34–41. [CrossRef]

56. Xu, Y.; Schoonen, M.A.A. The absolute energy positions of conduction and valence bands of selected semiconducting minerals. *Am. Mineral.* **2000**, *85*, 543–556. [CrossRef]
57. Heinemann, M.; Eifert, B.; Heiliger, C. Band structure and phase stability of the copper oxides Cu_2O, CuO, and CuO_3. *Phys. Rev. B* **2013**, *87*, 115111. [CrossRef]
58. Zhang, Q.; Zhang, K.; Xu, D.; Yang, G.; Huang, H.; Nie, F.; Liu, C.; Yang, S. CuO nanostructures: Synthesis, characterization, growth mechanisms, fundamental properties, and applications. *Prog. Mater. Sci.* **2014**, *60*, 208–337. [CrossRef]
59. Liu, T.; Liu, B.; Yang, L.; Ma, X.; Li, H.; Yin, S.; Sato, T.; Sekino, T.; Wang, Y. RGO/Ag_2S/TiO_2 ternary heterojunctions with highly enhanced UV-NIR photocatalytic activity and stability. *Appl. Catal. B Environ.* **2017**, *204*, 593–601. [CrossRef]
60. Yang, Y.; Xu, D.; Wu, Q.; Diao, P. Cu_2O/CuO Bilayered Composite as a High-Efficiency Photocathode for Photoelectrochemical Hydrogen Evolution Reaction. *Sci. Rep.* **2016**, *6*, 35158. [CrossRef]
61. Li, H.; Su, Z.; Hu, S.; Yan, Y. Free-standing and flexible Cu/Cu_2O/CuO heterojunction net: A novel material as cost-effective and easily recycled visible-light photocatalyst. *Appl. Catal. B Environ.* **2017**, *207*, 134–142. [CrossRef]
62. Gang, X.; Xi, Z.; Wanying, Z.; Shan, Z.; Haijia, S.; Tianwei, T. Visible-light-mediated synergistic photocatalytic antimicrobial effects and mechanism of Ag-nanoparticles@chitosan–TiO_2 organic–inorganic composites for water disinfection. *Appl. Catal. B Environ.* **2015**, *170–171*, 255–262. [CrossRef]